1-2021

Biofilm and Cell Adhesion Strength on Dental Implant Surfaces via the Laser Spallation Technique

James D. Boyd
University of Kentucky, james.boyd@uky.edu

Arnold J. Stromberg
University of Kentucky, stromberg@uky.edu

Craig S. Miller
University of Kentucky, craig.miller@uky.edu

Martha E. Grady
University of Kentucky, m.grady@uky.edu

Biofilm and Cell Adhesion Strength on Dental Implant Surfaces via the Laser Spallation Technique

Digital Object Identifier (DOI)
https://doi.org/10.1016/j.dental.2020.10.013

Notes/Citation Information
Published in *Dental Materials*, v. 37, issue 1.

DENTAL MATERIALS 37 (2021) 48–59

Available online at www.sciencedirect.com

ScienceDirect

journal homepage: www.intl.elsevierhealth.com/journals/dema

Biofilm and cell adhesion strength on dental implant surfaces via the laser spallation technique

J.D. Boyd[a], *A.J. Stromberg*[b], *C.S. Miller*[c,d], *M.E. Grady*[a,*]

[a] *Department of Mechanical Engineering, University of Kentucky, Lexington, KY, USA*
[b] *Department of Statistics, University of Kentucky, Lexington, KY, USA*
[c] *Department of Oral Health Practice, College of Dentistry, University of Kentucky, Lexington, KY, USA*
[d] *Department of Oral Health Research, College of Dentistry, University of Kentucky, Lexington, KY, USA*

ARTICLE INFO

Article history:
Received 12 December 2019
Received in revised form
2 October 2020
Accepted 6 October 2020

Keywords:
Biofilm
Adhesion
Titanium
Laser spallation
Streptococcus mutans
MG 63
Surface roughness
Implant
Adhesion index
Weibull analysis

ABSTRACT

Objective. The aims of this study are to quantify the adhesion strength differential between an oral bacterial biofilm and an osteoblast-like cell monolayer to a dental implant-simulant surface and develop a metric that quantifies the biocompatible effect of implant surfaces on bacterial and cell adhesion.

Methods. High-amplitude short-duration stress waves generated by laser pulse absorption are used to spall bacteria and cells from titanium substrates. By carefully controlling laser fluence and calibration of laser fluence with applied stress, the adhesion difference between *Streptococcus mutans* biofilms and MG 63 osteoblast-like cell monolayers on smooth and rough titanium substrates is obtained. The ratio of cell adhesion strength to biofilm adhesion strength (i.e., Adhesion Index) is determined as a nondimensionalized parameter for biocompatibility assessment.

Results. Adhesion strength of 143 MPa, with a 95% C.I. (114, 176), is measured for MG 63 cells on smooth titanium and 292 MPa, with a 95% C.I. (267, 306), on roughened titanium. Adhesion strength for *S. mutans* on smooth titanium is 320 MPa, with a 95% C.I. (304, 333), and remained relatively constant at 332 MPa, with a 95% C.I. (324, 343), on roughened titanium. The calculated Adhesion Index for smooth titanium is 0.451, with a 95% C.I. (0.267, 0.622), which increased to 0.876, with a 95% C.I. (0.780, 0.932), on roughened titanium.

Significance. The laser spallation technique provides a platform to examine the tradeoffs of adhesion modulators on both biofilm and cell adhesion. This tradeoff is characterized by the Adhesion Index, which is proposed to aid biocompatibility screening and could help improve implantation outcomes. The Adhesion Index is implemented to determine surface factors that promote favorable adhesion of cells greater than biofilms. Here, an Adhesion Index $\gg 1$ suggests favorable biocompatibility.

* *Corresponding author at*: 506 Administration Drive, Lexington, KY, 40506, USA.
E-mail address: m.grady@uky.edu (M.E. Grady).

https://doi.org/10.1016/j.dental.2020.10.013

1. Introduction

Dental implants are exposed to numerous oral bacteria, which can colonize the titanium surface leading to an infection called peri-implantitis. With infection rates as high as 28%, peri-implantitis is a serious problem in today's dental community [1]. Peri-implantitis stems from the adhesion and development of a colonized bacterial biofilm onto the subgingival implant surface [2]. Complications from biofilm formation are prolific in implantology, accounting for a quarter of all infections annually [3]. Even with the numerous advancements in the study of biomaterials, device-related infections remain a critical problem. To prevent these bacterial biofilms from forming, it is paramount to study and quantify the adhesion of bacteria onto various surfaces. Preventing the initial adhesion of pathogenic bacteria and biofilm formation would mark a significant step to deter bacterial infection of implants. Lack of available quantitative, high throughput, adhesion techniques hinders our progress toward optimal implant surface designs. Additionally, during implant design, biocompatibility assessments focus entirely on the implant-host response, omitting the impact of bacteria-implant-host response. An understanding of factors that contribute to strong biofilm surface adhesion at implant interfaces can guide the development of surfaces that prevent deleterious biofilms and promote osseointegration.

Unfortunately, there is still a large gap in knowledge of biofilm surface adhesion and the biocompatibility of implants, especially dental implants. Currently, the most ubiquitous bacterial adhesion technique is quantitative polymerase chain reaction (qPCR) [4,5]. Consistent enumeration is provided by qPCR, however, the technique lacks the ability to generate a quantified adhesion strength, which is related to force of removal. For example, atomic force microscopy (AFM), and jet impingement are two such critical force methods [6–10]. However, AFM is best suited to measure pull-off forces of a single bacterium or the agglomeration of a few bacteria. The size scale of an AFM tip precludes the collection of macroscopic pull off forces of a realistic magnitude, which limits the ability to measure macroscopic biofilm adhesion. Additionally, jet impingement is applied over the entire biofilm, suitable for testing a single film during loading. Deployment of jet impingement in an adhesion screening capacity across many surfaces would require many separate tests to accumulate reasonable repeatability. As such, an adhesion test with higher throughput than jet impingement would be advantageous to adhesive screening. The variety of testing methods also gives rise to a lack of consensus on the effects of surface roughness on bacterial adhesion. Some studies state that roughness increases adhesion [11,12], while other studies are unable to find a correlation [9,13]. The lack of consensus on the effects of surface roughness on adhesion limits the development of optimized implant surfaces. Another major problem with implant designs is there is no approach that directly compares the adhesion strengths of bacteria and cells on the same surfaces by the same technique. Several qualitative studies examine the impact of surface modifications on the number of bacteria or cells adhered to a surface [14–17]. However, comparing the quantities of bacteria to cells adhered to a surface provides little insight into any competition, as the number of bacteria which are adhered will greatly surpass that of cells. Current biocompatibility standards including ISO-10993, the biological evaluation of medical devices, does not prescribe the need for bacterial adhesion testing of implanted devices [18]. A direct comparison between cell adhesion to implant and biofilm adhesion to implant could aid in the bioassessments of implants by quantifying the tradeoffs among different surface parameters. A bioadhesion assessment that compares the adhesion of both bacteria and host cells onto implant surfaces is needed.

In this work, the laser spallation technique is employed to measure the adhesion differential between bacterial biofilms and osteoblast-like cells on implant mimicking surfaces. The laser spallation technique achieves macroscopic quantitative adhesion measurements through localized stress wave loading which permits multiple loading locations on the same film [19–22]. The laser spallation technique is implemented to compare the effect of implant surface characteristics on bacterial biofilm, and cell monolayer adhesion in order to obtain quantitative adhesion measurements of each biomaterial on rough and smooth titanium. Titanium roughnesses are chosen to mimic those found on commercially available dental implants. The adhesion measurements for both host cells and deleterious bacteria can be compared directly to obtain the Adhesion Index, the ratio of cell adhesion to biofilm adhesion, which we present for the first time.

The Adhesion Index is intended to be a quantitative metric for use in biocompatibility screening of medical implant surfaces. The initial stage of medical device implantation is the most vulnerable time for the development of bacterial infections [23,24]. As such, early colonizing and initial cell adhesion are the main focus for this study. Established growth protocols are used to test the baseline adhesion for both the bacterial biofilm model and the host cell model. A single-species biofilm of *Streptococcus mutans* is chosen as the bacterial biofilm, and MG 63 osteosarcoma cells are chosen as the cell monolayer. *S. mutans*, a Gram-positive bacterium, is a major etiological agent of human dental caries that colonizes the oral cavity and forms bacterial biofilms [25]. Moreover, *S. mutans* has been shown to stimulate the growth and adhesion of deleterious bacteria and has been used in prior oral biofilm adhesion studies [9,26,27]. MG 63 osteosarcoma cells display numerous osteoblastic traits that are typical of immature osteoblasts that would adhere during osseous integration with the dental implant [28,29]. Titanium is the current standard in the dental implant industry for many reasons such as its biocompatibility with bone and surrounding gum, high corrosion resistance, and its modulus of elasticity is comparable to that of bone [30]. Thus, commercially pure titanium is used to mimic the surface of a dental implant. Implant surfaces include roughened threading, to increase osseointegration, as well as unroughened surfaces. We selected both smooth titanium and rough titanium surfaces, with measured average roughness, Ra = 1.2 μm, which falls within the commercial standard range of Ra = 1–1.5 μm [13].

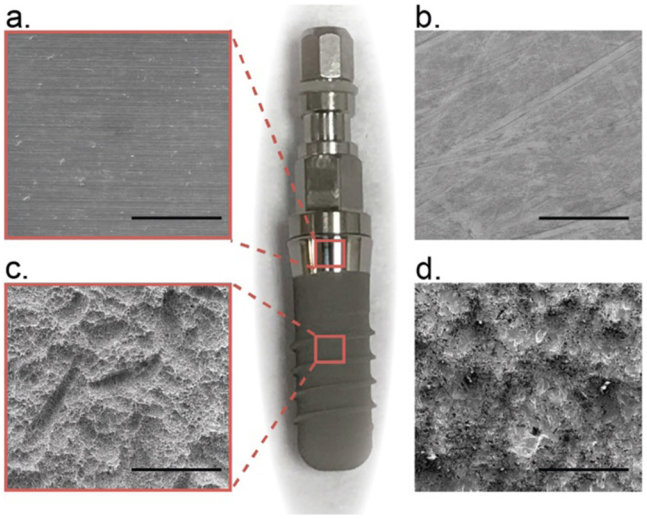

Fig. 1 – SEM images of (a,c) Straumann dental implant surface and (b,c) dental implant-mimicking surfaces used in this study. Scale bars are 100 μm.

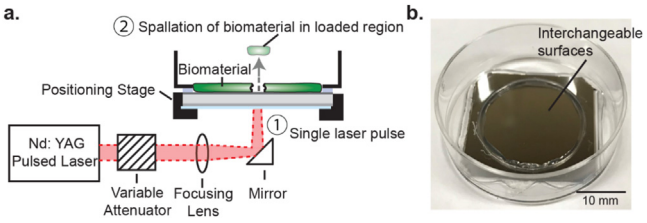

Fig. 2 – (a) Schematic of laser spallation setup used during experimentation where ① impingement of a single laser pulse ultimately initiates ② debonding of the biomaterial within the loaded region. (b) Substrate assembly before culture of test biomaterial.

2. Materials and methods

2.1. Substrate preparation

A complete substrate assembly is constructed to culture bacteria and cells while maintaining the integrity of the energy absorbing and confining layers needed for laser spallation [31]. Glass slides with one side coated with 100 nm of commercially pure titanium, 99.995% titanium, and the other side coated with 300 nm of aluminum are purchased from Deposition Research Laboratory Inc. (DRLI). The aluminum side of the sample is used as an absorbing layer for the Nd:YAG laser. A second set of slides are purchased from DRLI where the glass surface is sandblasted in order to achieve a uniform roughness of 1.22 μm, then coated in thermally evaporated titanium. To confirm roughness a white light ZYGO interferometer measured the Ra value for 5 slides, across 6 locations on those slides, resulting in an average 1.22 ± 0.08 μm roughness. Scanning electron microscope (SEM) images of the substrate assemblies are compared to the surfaces of a Straumann SLA dental implant in Fig. 1. Slides are cut into 1-inch × 1-inch squares and the aluminum layer is coated in a layer of sodium silicate (waterglass) (Fisher Chemical SS338-1) with a uniform thickness, 5.5 μm, using a Specialty Coatings System G3P-8. These substrates are then adhered to the bottom of 35 mm Petri dishes with precut holes, using vulcanizing bioinert silicone (Dowsil 732 Multi-Purpose Sealant).

2.2. Cell and biofilm culture

S. mutans (Wild type Xc) [32] is cultured in Todd Hewitt Yeast broth (THY). *S. mutans* is cultured until an OD_{600} of 0.7 is obtained. The bacterial solution is added into the Petri dish assemblies and diluted with a mixture of THY and 75 mM sucrose for a final OD_{600} of 0.175. Inoculated substrate assemblies are cultured at 37 °C with 5% CO_2 and cultured for 24 h. Media is removed and the biofilms are gently rinsed with phosphate buffered saline (PBS) in order to remove any bacteria not colonized within the biofilm.

MG 63 cells (ATCC CRL-1427) are cultured inside a cell culture flask with Eagle's Minimum Essential Medium (EMEM, ATCC 30-2003), 10% fetal bovine serum (FBS, ATCC 30-2020), 1% penicillin streptomycin solution (ATCC 30-2300) until confluent. The cells are then trypsinized and placed into an automatic cell counter. Cell concentrations of 120k are then placed inside the Petri dish assemblies with more EMEM solution and incubated at 37 °C with 5% CO_2 for 48 h, until confluent. Bacteria and cells are cultured separately onto our substrate assemblies before stress wave loading occurs. Immediately before testing, the culture media is aspirated and the films are rinsed with PBS to ensure the films are still hydrated during testing, and do not dry out. After stress wave loading, biofilms and cells are dyed using Syto-9 (Thermo Fisher Scientific S34854) and Calcein AM (Thermo Fisher Scientific L3224), respectively, in order to determine attachment of the surrounding cells. Fluorescence staining by Syto9 is also used to determine biofilm thickness. After staining, biofilms are then imaged using a Zeiss LSM 880 NLO upright confocal microscope. Z-stacks are collected using the Nyquist function native to the confocal which optimizes the number of slices needed per sample. Z-stack images are then analyzed in biofilm thickness software, Imaris. The biofilms cultured on smooth titanium had an average thickness of 21.4 ± 0.61 μm, and biofilms cultured on roughened substrates had an average thickness of 25.6 ± 1.02 μm, across 6 samples, respectively.

2.3. Laser spallation configuration and film loading

The laser spallation experimental setup used during biofilm and cell-substrate adhesion measurements is shown schematically in Fig. 2a. An Nd:YAG laser pulse of 10 ns duration, wavelength of 1064 nm, with adjustable energy from 0 to 300 mJ, is used to obtain film spallation. A laser pulse is focused to a 2.2 mm spot size and reflected to impinge upon the backside of the substrate. Upon absorbing the laser energy, the sudden expansion of the absorbing layer generates a compressive stress wave that propagates towards the film on the front surface of the substrate. The wave then reflects at the thin film free surface resulting in a tensile load onto the biomaterial-titanium interface. Though localized heating will occur, the rapid onset of the acoustic wave causes spallation to initiate before heat can impact relevant cells. Additionally,

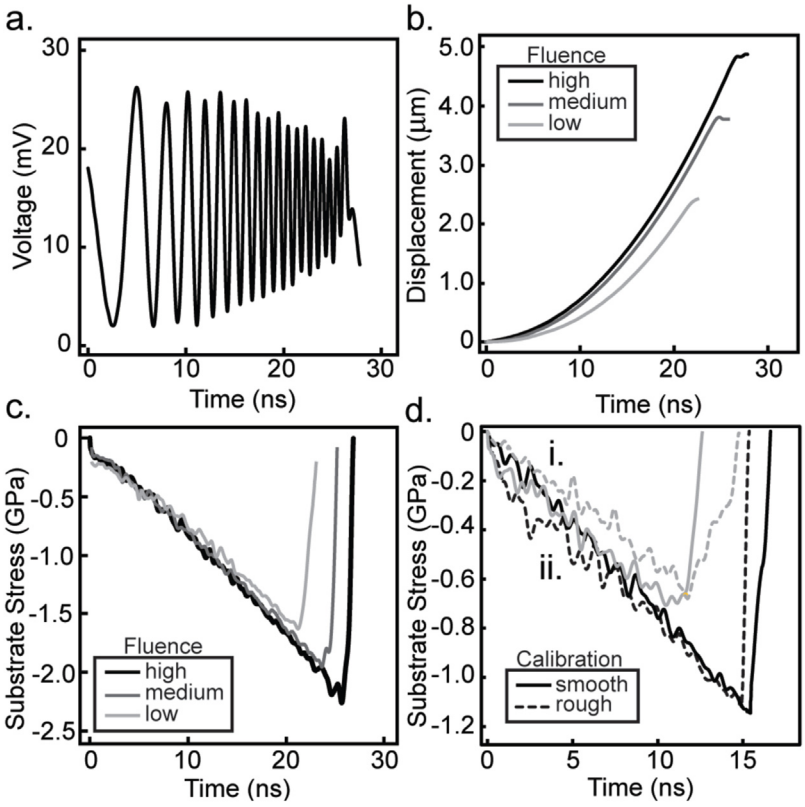

Fig. 3 – Raw data is shown for (a) a typical voltage curve recorded during calibration experiments at a high fluence, (b) the temporal displacement at a low, medium, and high fluence, and (c) the associated substrate stress profiles calculated for the low, medium, and high fluences. Low, medium, and high fluences correspond to 39.7, 55.6, and 79.4 mJ/mm^2, respectively. Substrate stress profiles in (d) demonstrate the similarity between calibration experiments on rough (dashed line) and smooth (solid line) substrates at a fluence of (i) 55.6 mJ/mm^2 in gray and (ii) 79.4 mJ/mm^2 in black.

a gap the size of a single loaded region is kept between each loading to ensure that any heat or acoustic wave would have little to no impact on subsequent loading locations.

Each substrate assembly is loaded at multiple locations by adjusting appropriate translation stages. The substrate assembly, depicted in Fig. 2b, and the experimental method of spallation testing are discussed in greater detail in Boyd et al. [31] and Kearns et al. [21]. During spallation testing both biofilm and cell monolayers are loaded over a range of fluences (7.93–79.4 mJ/mm^2), which corresponds to 12–15 loading locations per test film. The experiment is repeated 12 times for each of the four conditions: *S. mutans* biofilm on smooth titanium, *S. mutans* biofilm on roughened titanium, MG 63 cells on smooth titanium, and MG 63 cells on roughened titanium. Overall, over 100 loaded regions are examined for each film, to determine fluence of failure. Failure is recorded when visible concentric ejection of the film at the loaded region is observed. The failure rate of each condition at each fluence is recorded, which is used to calculate the half-life and quantify adhesion strength.

2.4. *Stress wave calibration*

Stress wave calibrations are performed to convert laser energy to loading stress. Because biofilms and cells are nonreflective, in situ calibrations are precluded. Instead, calibration experiments are performed directly on unmodified substrate assemblies following previously described protocols [22,33,34]. At each laser fluence, laser impingement and subsequent stress wave loading causes the surface of the substrate assembly to displace. These surface displacements are measured with a Michelson interferometer that includes a 532 nm continuous wave laser. Because the loading is rapid, over tens of nanoseconds, traditional displacement measurement devices are inadequate. A high rate oscilloscope (LeCroy WaveRunner 8404 M) records the temporal voltage trace from the Michelson interferometer via a silicon photodetector (Electo Optics ET 2030). The voltage curve can be described by the equation,

$$V(t) = \frac{V_{max} + V_{min}}{2} + \frac{V_{max} - V_{min}}{2}(\sin(2\pi n(t))) \quad (1)$$

where V(t) is the voltage, V_{max}, and V_{min}, are the voltage maximum and minimum, and n(t) is the fringe number. From the voltage trace, the fringe number n(t) is unwrapped and converted to displacement, u(t), using (Eq. (2)) and the wavelength of the interferometric laser, λ_0 = 532 nm [35].

$$u(t) = \frac{\lambda_0 n(t)}{2} \quad (2)$$

An example voltage trace for a single fluence and the corresponding displacement at that fluence alongside displacements for two other fluence values is illustrated in Fig. 3a,b. In Fig. 3b, lower fluence values result in less displacement when compared to the displacement of the higher fluence, which is expected. For the example fluence values of 39.7, 55.6, and 79.4 mJ/mm^2, found in Fig. 3, the resulting maximum displacement for these voltage curves is 2.39, 3.59, and 4.71 μm, respectively. For a simple bi-material interface, the evolution of the substrate stress can easily be determined from the displacement history using the principles of one-dimensional wave mechanics [33]. Thus, using the displacement history, density of material ρ, and speed of sound through the material, C_d, the substrate stress profile, σ_{sub}, is obtained by Eq. (3).

$$\sigma_{sub} = -\frac{1}{2}(\rho C_d)_{sub}\frac{du}{dt} \tag{3}$$

Fig. 3c contains the substrate stress profiles obtained for the same three displacement profiles shown in Fig. 3b. An increase in laser fluence results in an increase in peak substrate stress. For fluence values of 39.7, 55.6, and 79.4 mJ/mm^2, the example resulting peak substrate stresses are 1.51, 2.15, and 2.26 GPa, respectively. The slope of the loading substrate stress profile, i.e., the slope in the first 20 ns, for each fluence overlap each other, this result is expected since the slope is determined by the substrate material, glass in our case.

In order to perform calibration experiments on the roughened titanium, thin cover slips, 170 μm thickness (VWR micro cover glass No. 2), are adhered to the surface with Norland 60 Optical Adhesive and then coated in 150 nm of aluminum by Lesker physical vapor deposition (PVD) [36]. The same procedure is performed on smooth titanium substrates and the substrate stress profiles are compared in Fig. 3d. The shapes of the measured stress pulses show good agreement at each laser fluence. Peak substrate stress amplitude is equal at all fluences tested, varying by less than one standard deviation from the smooth titanium calibrations. Thus, the substrate stress profiles revealed that the rough surface had little to no measurable impact on wave propagation and thus smooth titanium is used for accurate stress wave calibration [36]. By performing a set of calibration experiments, the peak substrate stress at each fluence tested is measured and shown in Fig. 4 as average and standard deviation of triplicate measurements.

Following the protocol developed by Kandula et al. [33] a modified equation for peak interface stress, $\sigma_{int,peak}$, is derived using wave transmission and reflection coefficients,

$$\sigma_{int,peak} = -\frac{4\alpha_I}{(1+\alpha_I)^2}\sigma_{sub,peak} \tag{4}$$

where α_I is equal to the ratio of the acoustic impedance, defined as the density times the dilatational wave speed, for the biofilm and titanium substrate, given as,

$$\alpha_I = \frac{\rho_2 C_2}{\rho_1 C_1} \tag{5}$$

The density and dilatational wave speed of cells and bacteria for our calculations are assumed to be that of water, 997 kg/m^3 and 1500 m/s, respectively, consistent with the works of other biomaterial researchers [37,38]. The density and dilatational wave speed for commercially pure titanium are 4506 kg/m^3 and 6070 m/s, respectively. Through replacement of ρ_1 = 4506 kg/m^3, ρ_2 = 997 kg/m^3, C_1 = 6070 m/s, and C_2 = 1500 m/s into Eq. (5) and substitution of α_I into Eq. (4), we obtain:

$$\sigma_{int,peak} = -0.181\sigma_{sub,peak} \tag{6}$$

Thus, the peak interface stress is directly related to the peak substrate stress measured experimentally and determined by the loading laser fluence.

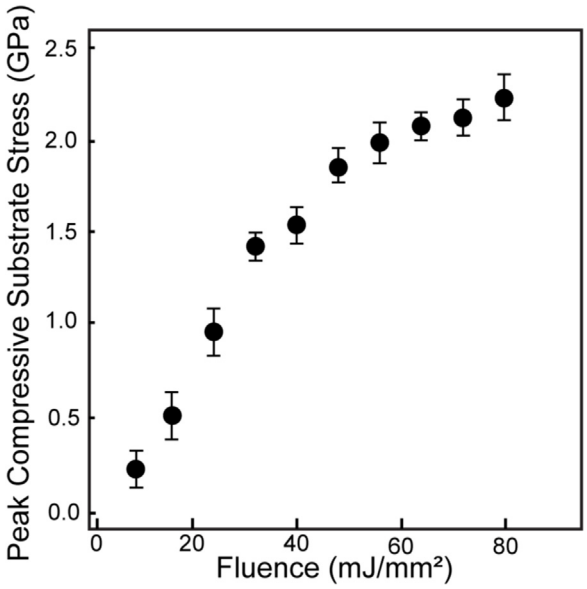

Fig. 4 – Average peak compressive substrate stress measured at increasing laser fluence during spallation experiments. Error bars represent one standard deviation.

3. Results

3.1. *Stress wave loading of biological films induces concentrated film ejection*

S. mutans biofilms and MG 63 monolayers are loaded using the laser spallation technique. The loading results in concentrated film ejection while leaving surrounding cells adherent. The failure progression of each film tested is represented in Fig. 5. Images in Fig. 5 row 1 are from unloaded regions of each film. Fig. 5 row 2 and 3 include images of loading locations at a fluence of 39.7 mJ/mm^2 and 79.4 mJ/mm^2, respectively. Loading of MG 63 cells on smooth titanium at 39.7 mJ/mm^2, row 2 column 1, results in film ejection while MG 63 cells on rough titanium at the same fluence, row 2 column 2, results in minimal film disturbance. Since the applied loading stress is the same at the same fluence, the difference in film failure is a direct result of the difference in adhesion strength. When comparing biofilm adhesion at the same fluence of 39.7 mJ/mm^2, row 2 column 3–4, there is no film ejection. This difference indicates *S. mutans* biofilms have greater adhe-

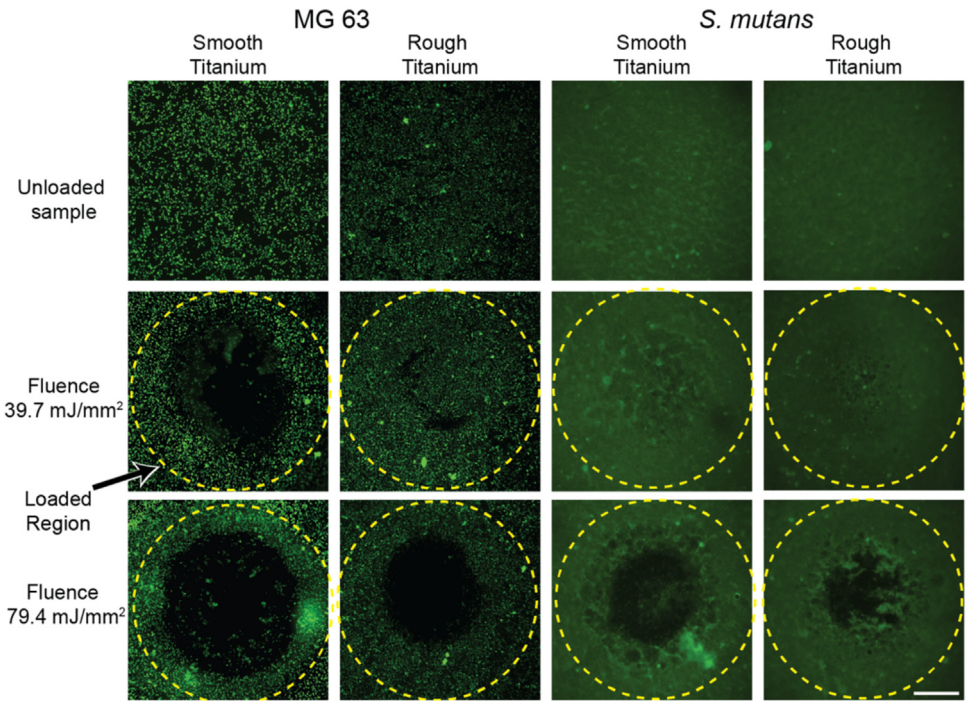

Fig. 5 – Fluorescence microscopy of MG 63 cell monolayers (first two columns from the left) and *S. mutans* biofilms (last two columns) of an unloaded region (first row from top), a loaded region at a fluence of 39.7 mJ/mm^2 (second row), and a loaded region at a fluence of 79.4 mJ/mm^2 (third row). Yellow dashed line indicates the loaded region, 2.2 mm diameter. MG 63 cell monolayers and *S. mutans* biofilms are stained with Calcein AM, and Syto 9, respectively. Scale bar is 0.5 mm (For interpretation of the references to colour in this figure legend, the reader is referred to the web version of this article).

sion than MG 63 cell monolayers. Qualitatively, we found no noticeable effect on film failure for *S. mutans* biofilms on either smooth or rough substrates. At very high laser fluences, all films experience localized ejection (e.g., Fig. 5 row 3) while maintaining attachment of the surrounding cells.

3.2. *Adhesion strength determined by half-life failure statistics*

Calibration experiments outlined in Section 2.4 convert laser fluence values into interface stress for *S. mutans* and MG 63 monolayers. Failure statistics recorded at each fluence across all replicates are plotted (Fig. 6) to determine the adhesion strength of each film. In uniform homogenous films, the dichotomic presentation of film failure makes adhesion strength readily determined. However, the onset of film ejection, termed spallation, occurs over a range of loading values instead of a single distinct interface stress for biological films. For example, in Fig. 6b, at an interface stress of 93.6 MPa, approximately 19% of MG 63 cell monolayers on smooth titanium failed, while at an increased stress of 256 MPa, 89% failed. Biofilms grown on rough titanium exhibited a narrower onset of spallation and approached a more dichotomic relationship. The failure statistics, $F(\sigma_{int,peak})$, are fit to a two parameter cumulative Weibull distribution function [39] (Eq. (7)). Weibull analysis, common in macroscopic adhesion analyses [9,40], calculates the half-life from a Weibull distribution, which is used as the adhesion strength, similar to the protocol developed by Grady et al. [22].

$$F\left(\sigma_{int,peak}\right) = 1 - e^{-\left(\frac{\sigma_{int,peak}}{\alpha}\right)^{\beta}} \quad (7)$$

The Weibull parameters, α and β, varied for each film condition and are included in Table 1 as well as the root mean square (RMS) difference between the experimental data and the Weibull model. Weibull parameters are optimized to the lowest RMS value. The Weibull model is interpolated to obtain the median value, the half-life, which represents the adhesion strength. Due to low RMS difference between the experimental film failure data and the Weibull model for *S. mutans* on rough titanium, asymptotic confidence intervals are unrealistically small, thus variability in both film failure data and calibrated interface stress were incorporated by using percentile bootstrap estimates by resampling both interface stress and film failure data simultaneously 1000 times. The 95% Confidence Intervals, 95% C.I., obtained from the 1000 iterations represent the range of plausible values wherein the true median lies. This procedure incorporates the experimental error represented by the horizontal error bars in Fig. 6 into the confidence interval for the median of the Weibull curve.

3.3. *S. mutans biofilms exhibit higher interface adhesion strength than MG 63 osteoblast-like cells*

Adhesion of *S. mutans* on smooth titanium is much greater than adhesion of MG 63 cells on smooth titanium. A qualita-

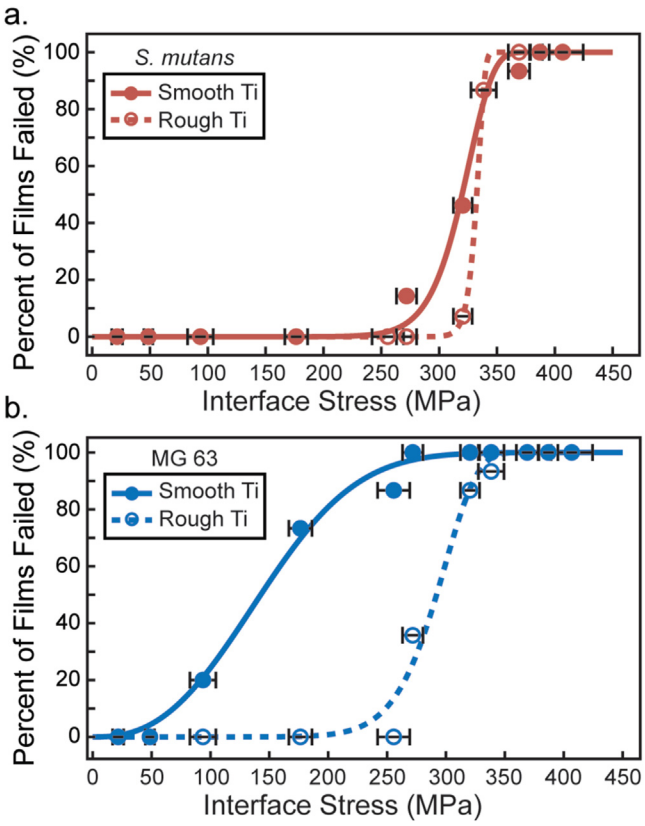

Fig. 6 – Failure statistics for (a) *S. mutans* biofilms on smooth titanium (solid red circles) and on rough titanium (open red circles) and (b) MG 63 cells on smooth titanium (solid blue circles) and on rough titanium (open blue circles) at increasing interface stress. Weibull models (smooth and dashed lines) are applied to interpolate the adhesion strength at a half-life of 50% failure. Error bars are the standard deviation of the calibrated interface stress at each point (For interpretation of the references to colour in this figure legend, the reader is referred to the web version of this article).

Table 1 – Adhesion strength for each film condition, corresponding Weibull parameters, and root mean square (RMS) difference between Weibull model and experimental data. Percentile bootstrap estimates are used to produce the 95% confidence intervals listed in parenthesis.

Film	Substrate	Adhesion strength (MPa)		α Parameter		β Parameter	RMS
S. mutans	Smooth	320	(304, 333)	327.1	(313.9, 337.6)	16.31 (9.07, 90.3)	0.0473
S. mutans	Rough	332	(324, 343)	334.5	(327.2, 343.0)	60.44(28.7, 473.6)	1.3e-6
MG 63	Smooth	143	(114, 176)	164.6	(129.2, 197.2)	2.57 (1.8, 28.6)	0.0382
MG 63	Rough	292	(267, 306)	301.3	(268.1, 314.8)	11.74 (7.9, 382.3)	0.0615

tive comparison of images before and after loading for each film type from Fig. 5 reveals that the onset of spallation begins at lower stresses for MG 63 monolayers on smooth titanium compared to *S. mutans*. Film spallation has already occurred for MG 63 monolayers at a fluence of 39.7 mJ/mm^2 (272 MPa), while no spallation is observed for *S. mutans* at the same loading magnitude. The disparity in adhesion becomes more evident with our quantitative analysis of failure statistics and Weibull model in Fig. 6. The onset of spallation for MG 63 monolayers occurs at loading stresses greater than 50 MPa and saturates at 100% failure at loading stresses greater than 272 MPa. In stark contrast, a loading stress of 50 MPa does not induce separation of *S. mutans* biofilms from smooth titanium substrates. Failure for *S. mutans* does not occur until loading stresses reach 272 MPa and saturates at 100% failure at 387 MPa. The half-life value is obtained from the median value of the Weibull model for each biomaterial and substrate combination. This half-life value is the adhesion strength and is plotted in Fig. 7. *S. mutans* biofilm adhesion strength is two-fold higher when compared to MG 63 cells adhesion strength on smooth titanium. MG 63 cells have an adhesion strength of only 143 MPa, with a 95% C.I. of (114,176), and *S. mutans* has an adhesion strength of 320, with a 95% C.I. of (304,333).

3.4. *Titanium surface roughness increases adhesion strength of MG 63 monolayers, but not S. mutans biofilms*

Similar to smooth titanium, the adhesion strength of *S. mutans* on roughened titanium is greater than MG 63 monolayers on roughened titanium, but MG 63 cells experience a greater increase in adhesion compared to *S. mutans*. This result appears qualitatively through a comparison of loaded regions.

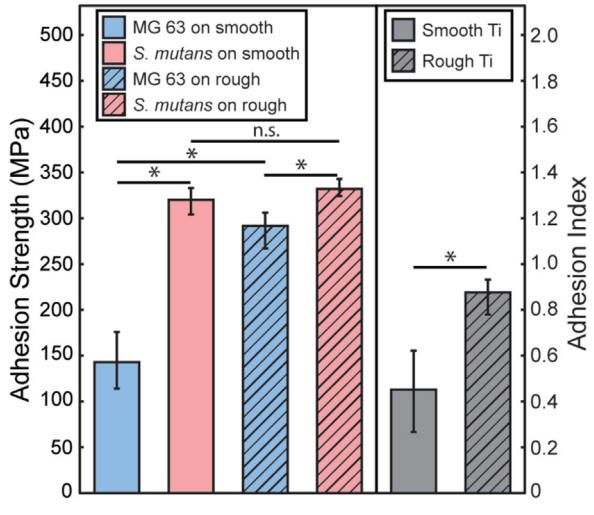

Fig. 7 – Adhesion strength for MG 63 cells (blue) and *S. mutans* (light red) biofilms on smooth (solid bars) and rough (hatched bars) surfaces. Surface roughness increases the adhesion for MG 63 cells with no effect on the adhesion strength of *S. mutans* biofilms. Adhesion Index, the ratio of MG 63 cells adhesion strength to *S. mutans* adhesion strength, is shown in grey for smooth and rough surfaces. Errors bars represent the 95% confidence intervals for all values. * $p < 0.05$ and n.s. not significant (For interpretation of the references to colour in this figure legend, the reader is referred to the web version of this article).

For example, in Fig. 5 columns 2 and 4, images of MG 63 cells have very small regions where cells have ejected, whereas images of *S. mutans* show no film ejection. However, when comparing columns 2 and 4 with the images taken on smooth titanium, columns 1 and 3, a greater difference in spallation regions is observed for MG 63 monolayers. Additionally, when examining the failure statistics, the onset of failure for MG 63 monolayers drastically increases from 93.6 MPa on smooth titanium to 272 MPa on rough titanium (Fig. 6). Whereas the onset of failure for *S. mutans* only increases from 272 MPa on smooth titanium to 320 MPa on rough titanium. The increase in surface roughness leads to an increase in adhesion strength for MG 63 cells from 143 MPa, with a 95% C.I (114, 176) on smooth titanium, to 292 MPa, with a 95% C.I. (267, 306) on rough titanium, and a slight, but not significant, increase in adhesion strength for *S. mutans* from 320 MPa, with a 95% C.I. (304, 333) on smooth titanium to 332 MPa, with a 95% C.I. (324, 343) on rough titanium. The increase observed for MG 63 cell monolayer adhesion is drastically higher than the increase observed for *S. mutans* biofilm adhesion onto roughened titanium. These changes in adhesion strength correspond to a 104% increase in adhesion strength of MG 63 monolayers and only a 4% increase for *S. mutans* biofilms when smooth titanium is replaced by rough titanium. Bootstrapped alpha values are used to compute p-values for testing pairwise differences in alpha values. A statistical difference is calculated when comparing the adhesion strength of MG 63 cells on smooth and rough titanium, p-value < 0.001, while no statistical difference is observed for the adhesion strength of *S. mutans* on smooth and rough titanium, p = 0.64. Additionally, the p-value when comparing the adhesion strength of MG 63 cells and *S. mutans* on rough titanium is p = 0.01. The level of significance indicates that the surface roughness greatly modifies adhesion strength for MG 63 monolayers, while no significant effect is found for *S. mutans* adhesion strength.

3.5. *Surface roughness increases the Adhesion Index of titanium*

In Section 3.4, we describe our finding that surface roughness affects adhesion of cell monolayers more than the adhesion of biofilms. To quantify the trade-off between increases in adhesion strength of cells and biofilms due to substrate modifications such as surface roughness, we developed the Adhesion Index. The ratio of the adhesion strength of cells (σ_{cell}) to the adhesion strength of biofilms ($\sigma_{biofilm}$) is the unitless Adhesion Index that describes which surfaces promote the adhesion of cells verses the adhesion of deleterious bacterial biofilms (Eq. (8)).

$$Adhesion\,Index = \frac{\sigma_{cell}}{\sigma_{biofilm}} \tag{8}$$

The adhesion strengths of both films are combined into the Adhesion Index using Eq. 8 and are plotted in Fig. 7. When bacteria and cells are cultured onto smooth substrates the Adhesion Index is measured at 0.451, with a 95% C.I. (0.267, 0.622). In comparison, the Adhesion Index increases to 0.876, with a 95% C.I. (0.780, 0.932) when they are cultured onto rough titanium substrates. Statistical comparison of the two Adhesion Index values yields a p-value < 0.002, indicating a statistically significant difference between the two values. It is apparent by examining the Adhesion Index that roughening the titanium surfaces has a greater impact on cell adhesion than biofilm adhesion.

4. Discussion

In this work, high-amplitude short-duration stress waves generated by laser pulse absorption are used to spall bacteria and cells from titanium substrates. The substrates upon which these films are cultured have been modified to directly compare the effect of macroscopic surface roughness on adhesion strength of the biological films.

The laser spallation technique has unique advantages for studying the macroscopic adhesion of biofilms due to its non-contact, localized, high strain-rate force applied to cause film ejection. The laser spallation technique has previously measured the adhesion of biological materials [31,41–43]. Some of these studies fail to calculate interface stress for the films of interest, thus no adhesion strengths are provided. The lack of calibration experiments eliminates direct comparison of adhesion values, except for the studies performed by Hagerman et al. and Nakamura et al. The former examined MC3T3 fibroblast cells plated on fibronectin (FN) coated and untreated polystyrene [42]. Adhesion of MC3T3 cells increased from 22.6 MPa on uncoated polystyrene to 34.9 MPa on FN coated polystyrene. Additionally, Nakamura et al. quantified the adhesion of bone marrow cells onto acid etched tita-

nium [43]. They found an increase in adhesion strength from approximately 175 MPa, to approximately 225 MPa. While values are expected to change based on cell type, surface, and culture conditions, the similar magnitudes measured between studies validate the laser spallation technique as a suitable biological film adhesion test. Additionally, the technique is suitable for parsing the minute differences that modifying implant surfaces can have on cellular and bacterial adhesion, especially when compared to existing non-quantitative adhesion tests.

Several studies have determined the improved osseointegration associated with increased surface roughness [28,44–46]. Implant surface roughness results in greater bone to implant contact and higher resistance to removal [47–50]. However, there is no general consensus on the effect of surface roughness on adhesion of bacteria. For example, Aykent et al. [11] and Duarte et al. [12], who studied *S. mutans* on dental resins, and *Streptococcus sanguinis* on titanium, respectively, report that increasing roughness results in increased adhesion. These studies employed counting methods to enumerate the presence of bacteria adhered to the surfaces. These results contrast directly with Mei et al. [9], who studied *S. sanguinis* on dental resins with atomic force microscopy, and indicated that surface roughness had no impact on bacterial adhesion. Similar roughness ranges of 1–2 μm were investigated in the previously mentioned studies. We believe the discrepancy within biomaterial adhesion studies of surface roughness is the result of at least three factors: (1) the use of a non-critical force adhesion measurement technique such as counting, (2) use of a micro or nanoscale adhesion technique to describe macroscale adhesive behavior or (3) the assumption that bacterial adhesion is the same as biofilm adhesion, which omits the contribution of biofilm EPS towards adhesion. The lack of consistency in bacterial adhesion studies impedes the design of implants and dental materials that deter bacterial adhesion, which could contribute to the significant rates of infection associated with orthodontics.

In this study, the quantitatively measured adhesion strength for MG 63 monolayers exhibited a statistically greater increase from smooth to rough titanium substrates, compared to *S. mutans*. This associated increase is readily quantified by examining the Adhesion Index. The Adhesion Index value nearly doubles from 0.451 on smooth titanium to 0.876 on rough titanium. If the bacterial adhesion to the titanium surface had increased due to roughness by the same fold, then the Adhesion Index would remain constant. Because of the drastic increase in cellular adhesion compared to bacterial adhesion we can assume that the roughened titanium surface in this study has a positive bio-adhesive impact on the dental implant surface. This increase is most likely associated with the differing size scale of cells and bacteria. The size of a single bacteria is on the order of single microns, the much larger cells are on the order of a hundred microns or more. Additionally, the EPS associated with *S. mutans* increases cohesion of the biofilm and adhesion of more virulent bacteria, but doesn't greatly increase surface adhesion [51]. Thus, the micron surface roughness increases the effective surface area of adhesion for cells on a length scale within a cell's grasp, while not impacting the initial bacterial surface adhesion.

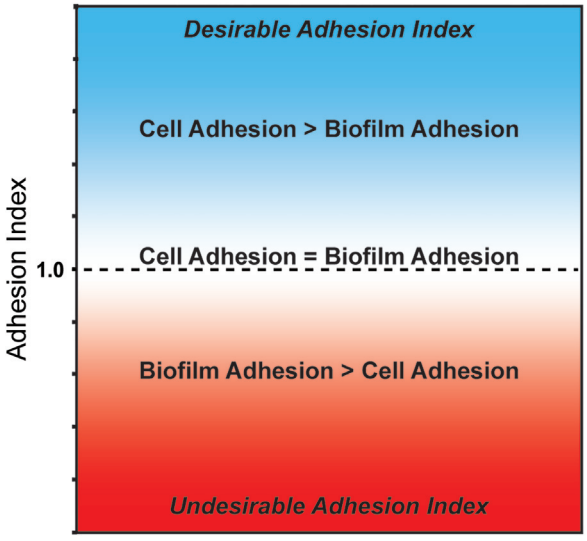

Fig. 8 – An ideal Adhesion Index demonstrates a much higher adhesion of mammalian cells than biofilms onto a surface. This result is mathematically written as an Adhesion Index ≫ 1.

The implementation of an Adhesion Index that directly compares the adhesion of host cells and deleterious bacteria, resulting in a nondimensional parameter, will help weigh the effects of surface modifications on the relative adhesion strength between cells and biofilms. Fig. 8 illustrates the guiding principles of the Adhesion Index. Values much less than one are undesirable as it indicates favoritism of bacterial biofilm adhesion. An Adhesion Index equal to one indicates that the adhesion strengths of cells and biofilms are equal. An Adhesion Index greater than one is desirable because that indicates the surface modification promotes cell adhesion over bacterial biofilm adhesion. While the precise optimal values for the Adhesion Index would need to be further studied, it is very useful when comparing two existing known surface morphologies to determine which is more likely to promote stronger cell adhesion than biofilm adhesion. Implementation of the Adhesion Index within our study indicates a more desirable Adhesion Index for roughened titanium over smooth titanium.

There are some limitations to this current study. This work presents a baseline Adhesion Index for a dental implant model of *S. mutans* and MG 63 cells on smooth titanium and a baseline Adhesion Index of the same dental model on rough titanium. Further studies should be conducted to determine target Adhesion Index values, currently the metric provides only a side-by-side comparison of material candidates. Additionally, the laser spallation technique precludes any co-culture experiments more common in biocompatibility, and current tests are in vitro and should seek to mimic in vivo conditions to accurately gauge implant response. Lastly, the use of wave transmission and reflection equations to calculate interface stresses means that final adhesion strength magnitude is controlled by use of accurate material properties, which are used to calculate the acoustic impedance.

5. Conclusions

In this study, the laser spallation technique is implemented to measure the adhesion strength of *S. mutans* biofilms and MG 63 cell monolayers on titanium surfaces. The laser spallation technique introduces a focused non-contact stress wave that detaches localized cells and captures the macroscopic adhesion effects for each film. The titanium surfaces selected simulate surfaces found on dental implants to determine the effects of surface roughness on adhesion strength. Biofilms of *S. mutans* and MG 63 cellular monolayers are cultured on smooth and rough titanium substrates. Each film-substrate combination is loaded using the laser spallation technique to determine failure statistics at increasing fluence values. Calibration experiments are performed using a Michelson type interferometer to record the free surface displacement during stress wave loading. Wave transfer equations are applied to calculate the interface stress at each loading fluence. Bootstrapping methods are applied to Weibull continuous distribution function curves to calculate the median, adhesion strength, value as well as the 95% confidence intervals. The ratio of adhesion strength values for *S. mutans* and MG 63 cells on the same substrates is calculated to obtain the Adhesion Index.

When titanium surface roughness increases, a significant increase in adhesion is measured for MG 63 monolayers, 143 MPa, with a 95% C.I. (114, 176), to 292 MPa, with a 95% C.I. (267, 306), while a significant change in *S. mutans* biofilm adhesion is not observed, 320 MPa, with a 95% C.I. (304, 333), to 332 MPa, with a 95% C.I. (324, 343). The adhesion values for MG 63 monolayers and *S. mutans* biofilms are directly compared to develop an Adhesion Index, which quantifies the adhesive competition between the bacteria and cells on an implant surface. The Adhesion Index for smooth titanium is calculated as 0.451, with a 95% C.I. (0.267, 0.622), and increases to 0.876, with a 95% C.I. (0.780, 0.932), for roughened titanium. The nondimensional parameter, the Adhesion Index, can help weigh the effects of surface modifications on the relative adhesion strength between cells and biofilms, and hopefully improve the efficacy of medical implant designs. The goal for this metric is to provide an additional predictor of a clinical outcome. This metric will supplement existing measurements, including cytotoxicity, to provide insight into the bacterial response associated with the designed implant surface.

The laser spallation technique allows for easily modified testing protocols, including different surface and culture conditions, as well as bacteria and cell selection. The substrate assembly dishes can be exchanged to examine a multitude of surfaces including other metals or even plastics and ceramics that might be used in the oral cavity (e.g., dental restoration composites, specialty coated implants) or in other permanent (e.g., hip, knee) or temporary (e.g., catheter, tube) implants. The biofilm-cell-surface model and culture conditions can be tailored to represent infections associated with implants in other locations. For example, *Staphylococcus aureus*, a rampant bacterial threat in the world of orthopedic implants [52], can be applied when examining hip and other fixative implants. Fibroblast cellular models can be applied to more dermal specific implants, such as catheters. Future work should expand the Adhesion Index to quantify the effect on adhesion for a variety of surfaces and using a multitude of bacterial and cell models.

Research data

The raw and processed data required to reproduce these findings are available to download from https://doi.org/10.18126/TW5W-XTWE [20] via the Materials Data Facility [54,55].

Acknowledgments

We gratefully acknowledge NIH Center of Biomedical Research Excellence(COBRE) in Pharmaceutical Research and Innovation (CPRI, P20GM130456),COBRE Phase III pilot funding (P30GM110788), andNIH NIDCR funding (R03DE029547) for completion of these experiments. SEM images were taken within the Electron Microscopy Center at the University of Kentucky by staff associate Nicolas Briot. Aluminum sputter coating was performed at The Micro/Nano Technology Center at University of Louisville and overseen by Dr. Thomas Berfield. We thank CPRI for use of bacterial culture equipment. CPRI is supported, in part, by the University of Kentucky College of Pharmacyand Center for Clinical and Translational Science (UL1TR001998). We thank Dr. Natalia Korotkova for her donation of *S. mutans* bacteria utilized during this study. We thank Dr. Larissa Ponomareva for sharing her culture expertise.

REFERENCES

[1] Schuldt Filho G, Dalago HR, Oliveira de Souza JG, Stanley K, Jovanovic S, Bianchini MA. Prevalence of peri-implantitis in patients with implant-supported fixed prostheses. Quintessence Int 2014;45(10):861–8.
[2] Rajiv Saini SS, Sharma Sugandha. Biofilm: a dental microbial infection. J Nat Sci Biol Med 2011.
[3] Arciola CR, Campoccia D, Montanaro L. Implant infections: adhesion, biofilm formation and immune evasion. Nat Rev Microbiol 2018;16(7):397.
[4] Yamane K, Ayukawa Y, Takeshita T, Furuhashi A, Yamashita Y, Koyano K. Bacterial adhesion affinities of various implant abutment materials. Clin Oral Implants Res 2013;24(12):1310–5.
[5] Garrett TR, Bhakoo M, Zhang ZB. Bacterial adhesion and biofilms on surfaces. Prog Nat Sci 2008;18(9):1049–56.
[6] Bayoudh S, Othmane A, Mora L, Ouada HB. Assessing bacterial adhesion using DLVO and XDLVO theories and the jet impingement technique. Colloids Surf B Biointerfaces 2009;73(1):1–9.
[7] Giliberti DC, Anderson KA, Dee KC. A jet impingement investigation of osteoblastic cell adhesion. J Biomed Mater Res 2002;62(3):422–9.
[8] Hallab N, Bundy K, O'Connor K, Clark R, Moses R. Cell adhesion to biomaterials: correlations between surface charge, surface roughness, adsorbed protein, and cell morphology. J Long Term Eff Med Implants 1995;5:209–31.
[9] Mei L, Busscher HJ, van der Mei HC, Ren Y. Influence of surface roughness on streptococcal adhesion forces to composite resins. Dent Mater 2011;27(8):770–8.

[10] Mehl C, Kern M, Schutte AM, Kadem LF, Selhuber-Unkel C. Adhesion of living cells to abutment materials, dentin, and adhesive luting cement with different surface qualities. Dent Mater 2016;32(12):1524–35.
[11] Aykent F, Yondem I, Ozyesil AG, Gunal SK, Avunduk MC, Ozkan S. Effect of different finishing techniques for restorative materials on surface roughness and bacterial adhesion. J Prosthet Dent 2010;103(4):221–7.
[12] Duarte PM, Reis AF, de Freitas PM, Ota-Tsuzuki C. Bacterial adhesion on smooth and rough titanium surfaces after treatment with different instruments. J Periodontol 2009;80(11):1824–32.
[13] Dos Santos MV, Elias CN, Cavalcanti Lima JH. The effects of superficial roughness and design on the primary stability of dental implants. Clin Implant Dent Relat Res 2011;13(3):215–23.
[14] Plaza D, Gallardo C, Straub Y, Bravo D, Pérez-Donoso J. Biological synthesis of fluorescent nanoparticles by cadmium and tellurite resistant Antarctic bacteria: exploring novel natural nanofactories. Microb Cell Fact 2016;15(1):76.
[15] Yoshinari M, Matsuzaka K, Inoue T. Surface modification by cold-plasma technique for dental implants—bio-functionalization with binding pharmaceuticals. Jpn Dent Sci Rev 2011;47(2):89–101.
[16] Al-Radha ASD, Dymock D, Younes C, O'Sullivan D. Surface properties of titanium and zirconia dental implant materials and their effect on bacterial adhesion. J Dent 2012;40(2):146–53.
[17] Kim M-H, Park K, Choi K-H, Kim S-H, Kim SE, Jeong C-M, et al. Cell adhesion and in vivo osseointegration of sandblasted/acid etched/anodized dental implants. Int J Mol Sci 2015;16(5):10324–36.
[18] Wallin RF, Upman P. A practical guide to ISO 10993-6: implant effects. Med Device Diagn Ind 1998;20:102–5.
[19] Gupta V, Argon A, Parks D, Cornie J. Measurement of interface strength by a laser spallation technique. J Mech Phys Solids 1992;40(1):141–80.
[20] Boyd JD, Miller CS, Grady ME. Biofilm and cell adhesion strength on titanium via the laser spallation technique. Mat Data Facility 2019, http://dx.doi.org/10.18126/TW5W-XTWE.
[21] Kearns KL, Boyd JD, Grady ME. Biofilm rupture by laser-induced stress waves increases with loading amplitude, independent of location. ACS Appl Bio Mater 2020;3(3):1426–33.
[22] Grady ME, Geubelle PH, Braun PV, Sottos NR. Molecular tailoring of interfacial failure. Langmuir 2014;30(37):11096–102.
[23] Ebersole JL, Dawson III D, Emecen-Huja P, Nagarajan R, Howard K, Grady ME, et al. The periodontal war: microbes and immunity. Periodontology 2000 2017;75(1):52–115.
[24] Pye AD, Lockhart DEA, Dawson MP, Murray CA, Smith AJ. A review of dental implants and infection. J Hosp Infect 2009;72(2):104–10.
[25] Krzysciak W, Jurczak A, Koscielniak D, Bystrowska B, Skalniak A. The virulence of *Streptococcus mutans* and the ability to form biofilms. Eur J Clin Microbiol Infect Dis 2014;33(4):499–515.
[26] Barbosa JO, Rossoni RD, Vilela SF, de Alvarenga JA, Velloso Mdos S, Prata MC, et al. *Streptococcus mutans* can modulate biofilm formation and attenuate the virulence of *Candida albicans*. PLoS One 2016;11(3):e0150457.
[27] Hahnel S, Rosentritt M, Burgers R, Handel G. Surface properties and in vitro *Streptococcus mutans* adhesion to dental resin polymers. J Mater Sci Mater Med 2008;19(7):2619–27.
[28] Chang YY, Huang HL, Chen YC, Hsu JT, Shieh TM, Tsai MT. Biological characteristics of the MG-63 human osteosarcoma cells on composite tantalum carbide/amorphous carbon films. PLoS One 2014;9(4):e95590.
[29] Bacakova L, Grausova L, Vacik J, Fraczek A, Blazewicz S, Kromka A, et al. Improved adhesion and growth of human osteoblast-like MG 63 cells on biomaterials modified with carbon nanoparticles. Diamond Relat Mater 2007;16(12):2133–40.
[30] Oshida Y. Bioscience and bioengineering of titanium material. 2nd edition Elsevier; 2013.
[31] Boyd JD, Korotkova N, Grady ME. Adhesion of biofilms on titanium measured by laser-induced spallation. Exp Mech 2019;59(9):1275–84.
[32] Edgar RJ, van Hensbergen VP, Ruda A, Turner AG, Deng P, Le Breton Y, et al. Discovery of glycerol phosphate modification on streptococcal rhamnose polysaccharides. Nat Chem Biol 2019;15(5):463–71.
[33] Kandula SSV, Hartfield CD, Geubelle PH, Sottos NR. Adhesion strength measurement of polymer dielectric interfaces using laser spallation technique. Thin Solid Films 2008;516(21):7627–35.
[34] Wang J, Weaver RL, Sottos NR. A parametric study of laser induced thin film spallation. Exp Mech 2002;42(1):74–83.
[35] Barker LM. Laser interferometry in shock-wave research. Exp Mech 1972;12(5):209–15.
[36] Boyd JD, Grady ME. The effect of surface roughness on laser-induced stress wave propagation. Appl Phys Lett 2020;117(12):121601.
[37] Paul E, Ochoa JC, Pechaud Y, Liu Y, Line A. Effect of shear stress and growth conditions on detachment and physical properties of biofilms. Water Res 2012;46(17):5499–508.
[38] Grover WH, Bryan AK, Diez-Silva M, Suresh S, Higgins JM, Manalis SR. Measuring single-cell density. Proc Natl Acad Sci U S A 2011;108(27):10992–6.
[39] Murthy DP, Xie M, Jiang R. Weibull models, vol. 505. John Wiley & Sons; 2004.
[40] van der Mei HC, de Vries J, Busscher HJ. Weibull analyses of bacterial interaction forces measured using AFM. Colloids Surf B Biointerfaces 2010;78(2):372–5.
[41] Hu L, Zhang X, Miller P, Ozkan M, Ozkan C, Wang J. Cell adhesion measurement by laser-induced stress waves. J Appl Phys 2006;100(8):084701.
[42] Hagerman E, Shim J, Gupta V, Wu B. Evaluation of laser spallation as a technique for measurement of cell adhesion strength. J Biomed Mater Res A 2007;82(4):852–60.
[43] Nakamura H, Shim J, Butz F, Aita H, Gupta V, Ogawa T. Glycosaminoglycan degradation reduces mineralized tissue–titanium interfacial strength, journal of biomedical materials research part A: an official journal of the society for biomaterials. Jpn Soc Biomater Aust Soc Biomater Korean Soc Biomater 2006;77(3):478–86.
[44] Shapira L, Halabi A. Behavior of two osteoblast-like cell lines cultured on machined or rough titanium surfaces. Clin Oral Implants Res 2009;20(1):50–5.
[45] Lincks J, Boyan BD, Blanchard C, Lohmann C, Liu Y, Cochran DL, Dean DD, Schwartz Z. Response of MG63 osteoblast-like cells to titanium and titanium alloy is dependent on surface roughness and composition. Biomaterials 1998;19(23):2219–32.
[46] Abraham CM. A brief historical perspective on dental implants, their surface coatings and treatments. Open Dent J 2014;8:50–5.
[47] Le Guéhennec L, Soueidan A, Layrolle P, Amouriq Y. Surface treatments of titanium dental implants for rapid osseointegration. Dent Mater 2007;23(7):844–54.
[48] Elias CN, Meirelles L. Improving osseointegration of dental implants. Expert Rev Med Devices 2010;7(2):241–56.
[49] Ehrenfest DMD, Coelho PG, Kang B-S, Sul Y-T, Albrektsson T. Classification of osseointegrated implant surfaces:

materials, chemistry and topography. Trends Biotechnol 2010;28(4):198–206.
[50] Anil S, Anand P, Alghamdi H, Jansen J. Dental implant surface enhancement and osseointegration, implant dentistry—a rapidly evolving practice; 2011. p. 83–108.
[51] Klein MI, Hwang G, Santos PH, Campanella OH, Koo H. *Streptococcus mutans*-derived extracellular matrix in cariogenic oral biofilms. Front Cell Infect Microbiol 2015;5:10.
[52] Li B, Webster TJ. Bacteria antibiotic resistance: new challenges and opportunities for implant-associated orthopedic infections. J Orthop Res 2018;36(1):22–32.
[54] Blaiszik B, Chard K, Pruyne J, Ananthakrishnan R, Tuecke S, Foster I. The materials data facility: data services to advance materials science research. JOM 2016;68(8):2045–52.
[55] Blaiszik B, Ward L, Schwarting M, Gaff J, Chard R, Pike D, et al. A data ecosystem to support machine learning in materials science. MRS Commun 2019;9(4):1125–33.